Kovacevic, N. *et al.* (2013). *Géotechnique* **63**, No. 9, 753–767 [http://dx.doi.org/10.1680/geot.12.P.066]

Finite-element analysis of the failure and reconstruction of the main dam embankment at Abberton Reservoir, Essex, UK

N. KOVACEVIC*, D. W. HIGHT*, D. M. POTTS† and I. C. CARTER‡

An existing 15·5 m high main dam embankment at Abberton Reservoir in Essex was completed in August 1938, since when its performance has been satisfactory. However, the upstream embankment shoulder of the original dam suffered a deep-seated failure through its foundation towards the end of construction in July 1937, 9 days before a similar and well-known failure occurred at Chingford Reservoir in close proximity to Abberton. Whereas the failure at Chingford became an important case in the history of soil mechanics through the involvement of Karl Terzaghi and marked one of the first applications of modern soil mechanics principles, the failure at Abberton has remained largely unknown, until recently when raising of the existing dam started to be considered. This paper describes advanced finite-element analyses which were carried out to investigate the failure of the original dam at Abberton and the stability of the existing main dam. The parameters used in the constitutive models were derived on the basis of the available site investigations and laboratory testing and on experience in the back-analysis of other failures in London Clay. The analyses demonstrated that the upstream shoulder of the original embankment failed through the mechanism of progressive failure, which involved the top of the stiff plastic London Clay rather than the overlying alluvium in the foundation. The relatively rapid rate of embankment filling, achieved by using modern earth-moving equipment, contributed significantly to the original dam failure. The analyses also demonstrated satisfactory behaviour of the existing dam during reconstruction, the first impounding and in the long term, with its response being similar to that observed. Thus the constitutive models used and parameters derived were successfully calibrated against the observed behaviour of both the original and existing main dams at Abberton, and could be used in predicting the behaviour of the dam during and after its proposed raising.

KEYWORDS: case history; dams; earthfill; failure; finite-element modelling; slopes

INTRODUCTION

Abberton Reservoir is situated on the Layer Brook, a tributary of the Roman River, 6 km south of Colchester in Essex (Fig. 1). It was formed by building an earthfill embankment (referred to hereafter as the main dam) across the valley, being 680 m long at the dam crest level. At its highest section, in the central part of the valley, the crest of the dam is some 15·5 m above the nominal ground level, which is approximately at El. +4 mOD. A typical cross-section of the existing main dam is shown in Fig. 2.

The embankment has a narrow central vertical core of puddle clay that extends below ground level in a cut-off trench through the underlying alluvium and into the in situ London Clay Formation (referred to as London Clay hereafter). The puddle clay core is approximately 1·5 m wide at its upper surface and widens with depth, having upstream and downstream faces of 1 to 15. Transition zones of selected clay fill were placed between the central clay core and outer portions of the upstream and downstream embankment shoulders. The dam shoulders were derived from the locally won sands and gravels (termed 'general' gravel).

Construction of the original dam started in March 1936 with an upstream slope of 1 (vertical) in 4 (horizontal), which suffered a deep-seated failure in July 1937 when the embankment was still some 2 m short of its full height (see Fig. 3). The slip involved a central section of the dam, approximately 175 m long (Fig. 4). Following the failure, the slipped material of the upstream shoulder and the central clay core were trimmed to about El. +9·0 mOD (see Fig. 3)

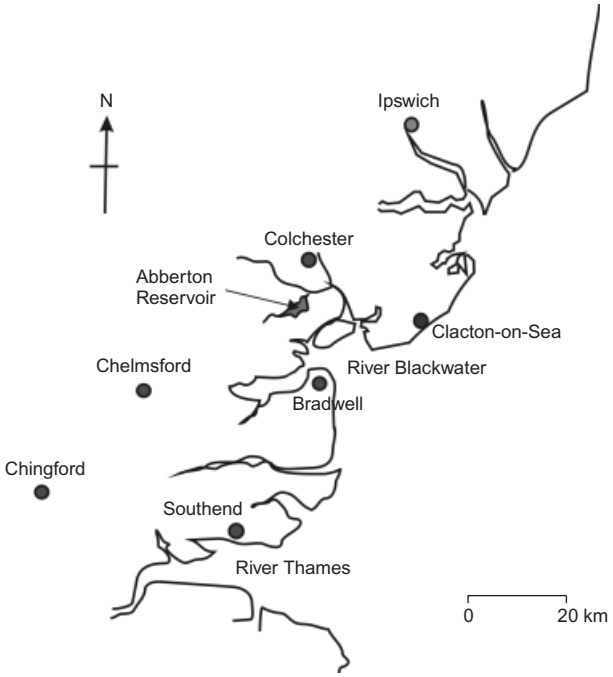

Fig. 1. Location of Abberton Reservoir (after French *et al.*, 2000)

Manuscript received 8 May 2012; revised manuscript accepted 5 September 2012. Published online ahead of print 4 December 2012. Discussion on this paper closes on 1 December 2013, for further details see p. ii.

* Geotechnical Consulting Group, London, UK.
† Imperial College, University of London, UK.
‡ MWH, High Wycombe, UK.

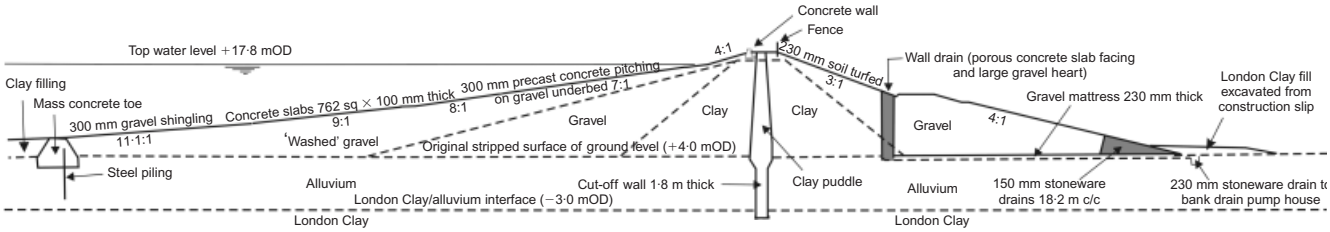

Fig. 2. Typical cross-section of main dam (after French *et al.*, 2000)

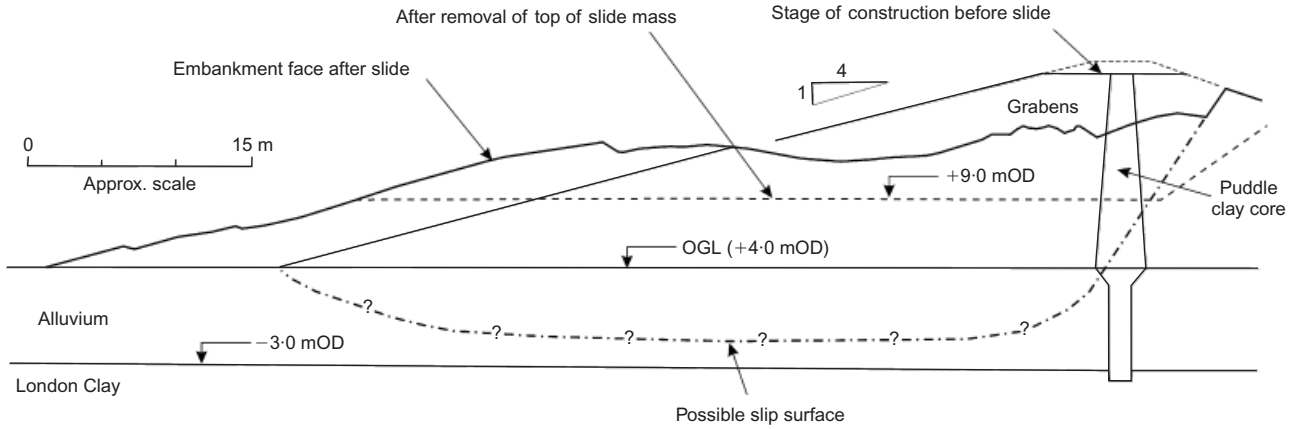

Fig. 3. Failed section of original dam (after Watson Hawksley, 1990)

Fig. 4. General view of original dam failure. At the time of collapse the embankment was about 13·5 m high, and the slip involved a 175 m long central section of the dam

and replaced with both clay and granular fill materials, forming a substantially flatter upstream slope of approximately 1 in 8·5. The outer portion of the reconstructed upstream shoulder was derived from partially washed gravels (termed 'washed' gravel). The dam has performed in a satisfactory manner since completion in August 1938. The settlement records are provided by Watson Hawksley (1990), whereas the available piezometer data are discussed by French *et al.* (2000).

The failure at Abberton occurred just 9 days before a similar failure during construction of Chingford embankment, again in Essex and in close proximity to Abberton (see Fig. 1). However, whereas the failure at Chingford was well documented (Cooling & Golder, 1942), and was subsequently recognised as a milestone in the early development of soil mechanics in the UK (Penman, 1986), the failure at Abberton remained largely unnoticed (French *et al.*, 2000). The purpose of this paper is to shed more light on the failure of the original dam at Abberton, and on the subsequent performance of the existing embankment. Both are relevant to the proposal to raise the existing dam by about 3 m.

GROUND INVESTIGATIONS, AND GROUND AND GROUNDWATER CONDITIONS

Ground investigations have been carried out at the site of Abberton main dam in connection with its proposed raising. Investigations in 1995 and 2007 involved boreholes, trial pits and cone penetration tests (CPTs), which were put down from the dam crest, from the downstream shoulder, and from near or beyond the downstream toe. The results of these investigations have been used to assess the properties of the in situ soils and of the construction materials, as described by GCG (2009).

The whole dam site at Abberton is underlain by the London Clay, which extends to about 25 m below the valley floor, where it overlies the Lambeth Group Formation. In the central part of the valley the London Clay is covered by a layer of alluvium approximately 7 m thick. The alluvium comprises soft and firm brown clay, white sandy clay, green clay, silt lenses or layers of sands and gravel. Peat layers are also common. Head covers the valley side slopes, and glacial drift and sand and gravel terrace deposits are found on the higher ground. There was no evidence of shear surfaces in the London Clay in the centre of the valley.

In the central part of the valley the observed groundwater table is close to the original ground level, and has been assumed in the analysis to be at ground level with a hydrostatic distribution of pore water pressures below.

In order to specify initial stresses in the ground (before construction of the original dam), and in the absence of site-specific investigations, it was necessary to make an assumption about the distribution of the coefficient of earth pressure at rest, K_0. A constant value of $K_0 = 0{\cdot}5$ was adopted in the alluvium, whereas calculations, following Burland *et al.* (1979) and taking into account the loading applied by the alluvium, indicated $K_0 = 1{\cdot}5$ in the London Clay. A transi-

tion between $K_0 = 0{\cdot}5$ and $1{\cdot}5$ was assumed over the top 5 m of the London Clay, which is likely to be weathered and disturbed by various periglacial processes in the past.

SOIL MODELS AND MODEL PARAMETERS

Before performing the finite-element (FE) analyses it was necessary to make the correct choice of constitutive models to characterise the behaviour of the various soils involved.

Soil models

The in situ London Clay is a stiff, heavily overconsolidated plastic clay, and as such is prone to the mechanism of progressive failure, with its strength reducing from peak to residual values due to strain-softening. In order to model the potential development of this mechanism it was decided to use a post-peak strain-softening constitutive model of the Mohr–Coulomb type, which has been successfully used in characterising the behaviour of various strain-softening materials in the past (see e.g. Vaughan *et al.*, 2004). The use of this constitutive model has been extensively calibrated for in situ London Clay in back-analyses of cut slope failures reported by Potts *et al.* (1997) and Kovacevic *et al.* (2004). Vaughan *et al.* (2004) back-analysed the Bradwell slip described by Skempton & LaRochelle (1965), which is particularly relevant, given its close proximity to Abberton in the east of the London Clay basin (see Fig. 1). The Mohr–Coulomb model, but without strain-softening, was also employed to characterise the behaviour of the various granular fills used in the construction of the dam. Both versions of the Mohr–Coulomb model are described in the Appendix.

The puddle clay of the narrow central core (and the cut-off trench) and selected clay fill in the transition zones were all derived from the London Clay borrow pits in the vicinity of the dam. Clay fills are remoulded, and it is known that the post-peak displacement on a discontinuity required to reduce their strength from peak to residual is greater than the in situ clays from which they are derived. This is because the bonded structure present in the in situ London Clay is progressively destroyed by excavation, placing and compaction. Thus the strain-softening behaviour of clay fills is likely to be of less importance than the strain-softening of the in situ clays from which they are derived, and in the analyses this aspect of the clay fills' behaviour was not modelled. Consequently, an elasto-plastic model of the critical state type (modified Cam Clay; see Roscoe & Burland, 1968) was used to characterise the pre-peak plastic behaviour of these materials, which was believed to be more important than the post-peak strain-softening.

Model parameters

The derived model parameters are listed in Table 1. Their derivation is briefly discussed below.

Puddle clay and transition clay fill. Whereas the London Clay used to form the puddle clay was placed at a moisture content well above the liquid limit, and was 'completely' remoulded, the London Clay for the transition fill was likely to have been placed at its natural moisture content, and spread and only lightly compacted by the earth-moving equipment used in the dam construction.

Given the different placing method used in practice, the analysis modelled the different undrained shear strength, S_u, operating in these fill materials immediately upon construction: $S_u = 10{\cdot}5$ kPa for the puddle clay core (Moffat, 2002)

Table 1. Material properties assumed in the analyses

Material property	Puddle clay*	Transition fill*	General gravel	Washed gravel	Clayey alluvium	Silty alluvium	In situ London Clay
Unit weight: kN/m^3	19	18	20	20	18	18	19·5
Effective stress strength parameters	$\phi'_{crit} = 21°$	$\phi'_{crit} = 23°$	$c' = 1$ kPa $\phi' = 35°$ $\psi = 10°$	$c' = 1$ kPa $\phi' = 35°$ $\psi = 10°$	$c' = 5$ kPa $\phi' = 20°$ $\psi = 0°$	$c' = 3$ kPa $\phi' = 30°$ $\psi = 0°$	$c'_{peak} = 8$ kPa $\phi'_{peak} = 24°$ $c'_{res} = 2$ kPa $\phi'_{res} = 13°$ $\psi = 0°$
Stiffness parameters	$\lambda = 0{\cdot}113$ $\kappa = 0{\cdot}030$ $\mu = 0{\cdot}30$	$\lambda = 0{\cdot}113$ $\kappa = 0{\cdot}030$ $\mu = 0{\cdot}30$	$E = 200p'$ (kPa) $E_{min} = 5$ MPa $\mu = 0{\cdot}20$	$E = 200p'$ (kPa) $E_{min} = 5$ MPa $\mu = 0{\cdot}20$	$E = 65p' + 5200$ (kPa) $\mu = 0{\cdot}30$	$E = 65p' + 5200$ (kPa) $\mu = 0{\cdot}30$	$E = 5000(p' + 100)/100$ (kPa) $\mu = 0{\cdot}20$
Permeability parameters, k: m/s	$3{\cdot}0 \times 10^{-11}$	$1{\cdot}0 \times 10^{-9}$	–	–	$1{\cdot}0 \times 10^{-8} e^{-0{\cdot}002p'}$	$1{\cdot}0 \times 10^{-7}$	$5{\cdot}0 \times 10^{-10} e^{-0{\cdot}007p'}$

* Specific volume at $p' = 1$ kPa is $v_1 = 1 + e_1 = 2{\cdot}5$.
Note: For in situ London Clay, effective stress shear strength parameters are reducing from peak values (c'_{peak} and ϕ'_{peak}) at $\varepsilon^p_{D,peak} = 5\%$ to residual values (c'_{res} and ϕ'_{res}) at $\varepsilon^p_{D,res} = 20\%$, where ε^p_D is the plastic shear strain invariant, defined in equation (10).

and $S_u = 30$ kPa for the transition clay fill. In the analysis, this was achieved by specifying a different amount of suction, S, in the 'newly' constructed layers of clay fill: $S = 50$ kPa for the puddle clay core and $S = 125$ kPa for the transition clay fill. It should be noted that samples of both these materials exhibit contractive behaviour during undrained shearing in isotropically consolidated triaxial compression tests, and they were therefore modelled as being normally consolidated upon their placing. A higher critical effective angle of shearing resistance, ϕ'_{crit}, was adopted for the transition clay fill than for the puddle clay core, on the basis of there being fewer lower-strength shear surfaces in the less heavily worked transition fill.

A comparison of the predicted and measured (or deduced) current undrained shear strengths is shown in Figs 5 and 6 for the puddle clay core and transition clay shoulder fill respectively. Making no allowance for arching effects in the core, and subtracting the full overburden stress from q_c, requires a cone factor, N_k, of 14·3 to provide a reasonable fit to the profile of S_u found in the unconsolidated undrained (UU) triaxial compression tests on the puddle clay (Fig. 5). Allowing for the effects of arching, the N_k factor would be higher. The current undrained strength in the core appears to increase with depth from approximately 20 kPa at the top, ignoring the possible effects of any drying, to 30 kPa at the base. The predicted long-term undrained strengths for the core in the FE analysis are lower at depths less than 15 m, but are more representative of the undrained strength at slower shearing rates.

The results of standard penetration tests (SPT), of UU triaxial compression tests on U100 samples and of vane tests on the transition clay fill are plotted against depth in Fig. 6. A correlation of $S_u = 5N$ has been assumed, where N is the SPT blow count. A lower bound to the strength data suggests a current undrained strength in the clay transition fill of 30 kPa to a depth of approximately 5·5 m, increasing to 75 kPa at approximately 14 m depth. The predicted long-term undrained strengths for the transition fill in the FE analysis are towards this lower bound of the measurements.

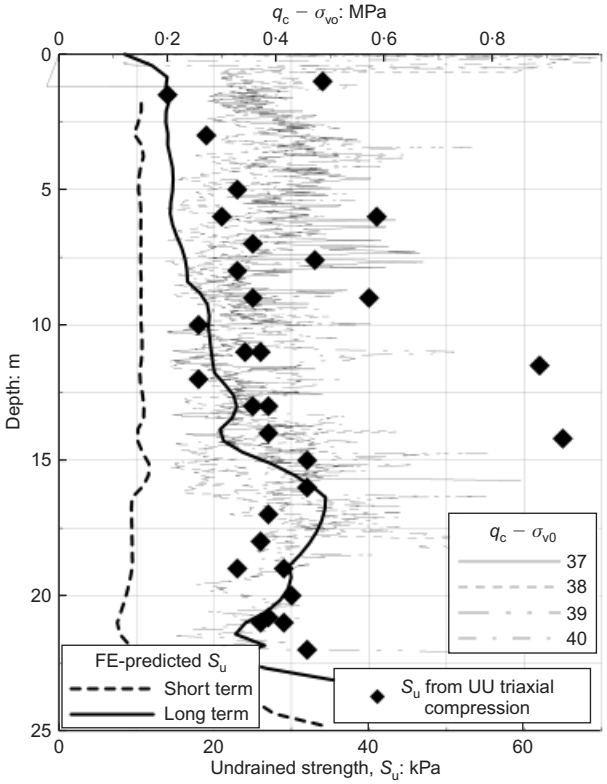

Fig. 5. Observed and predicted undrained strength in central puddle clay core of existing embankment

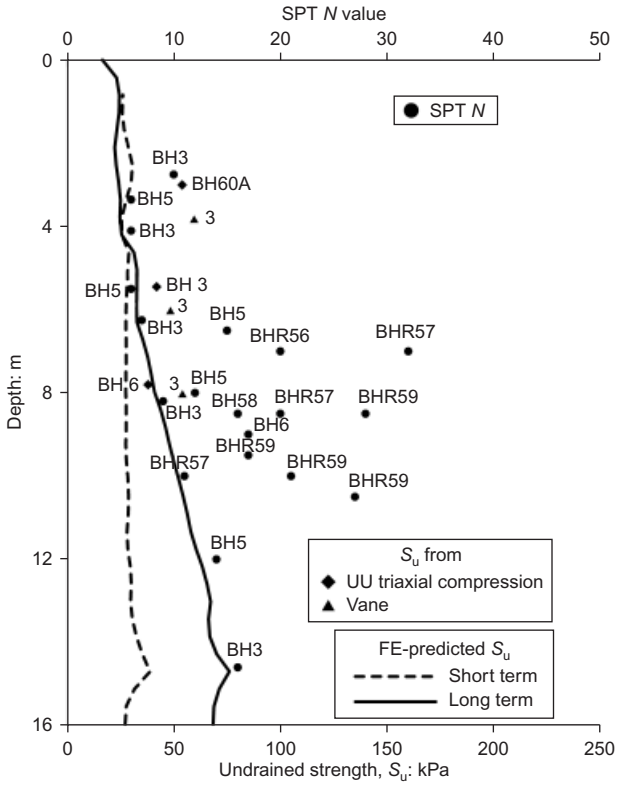

Fig. 6. Observed and predicted undrained strength in transition shoulder fill of existing embankment

Triaxial tests on samples of the puddle clay consistently indicated a very low permeability (the coefficient of permeability being in the order of $k = 10^{-11}$ m/s). However, similar tests showed that the permeability of the transition fill was substantially higher ($k = 10^{-6}$ to 10^{-7} m/s). Given the clayey nature of the transition fill, these permeability values were believed to be unrealistically high, and consequently a more credible value for the coefficient of permeability was adopted for the transition fill: $k = 10^{-9}$ m/s. This was confirmed independently by a parametric study in which the coefficient of permeability for the transition fill was progressively decreased until the observed pore water pressures downstream from the puddle clay core and cut-off trench (see French *et al.*, 2000) were reasonably matched by the analysis (see Fig. 20).

Granular shoulder fill. The granular fills used in construction of the dam were assumed to behave in a drained manner. The effective strength and stiffness parameters used in the non-linear elastic perfectly plastic Mohr–Coulomb model were derived from the SPT data presented in the GCG (2009) report, using correlations suggested by Clayton (1995). No distinction was made between the 'general' and 'washed' gravels.

Alluvium. The alluvium forms the top of the foundation in the centre of the valley to a depth up to 7 m. Although it is quite variable, detailed inspection of the CPT data has shown that the alluvium can generally be divided into two distinct deposits: the top, more clayey layer and the bottom, more silty one. In the FE analyses the clayey alluvium was assumed to be weaker and less permeable than the silty

alluvium beneath. No distinction was made between these materials as far as compressibility was concerned.

Triaxial compression tests on isotropically consolidated samples of alluvium gave peak drained strength parameters for the clayey alluvium of $c'_{peak} = 5$ kPa and $\phi'_{peak} = 20°$, and for the silty alluvium of $c'_{peak} = 3$ kPa and $\phi'_{peak} = 30°$ (see Fig. 7).

The laboratory test data suggest that the permeability of the clayey alluvium reduces with an increase in effective stress. To capture this observed behaviour, a non-linear permeability model (Vaughan, 1994) was adopted in the FE analyses. There is a lack of permeability data related to the silty alluvium, although its permeability is certainly higher than that of the clayey alluvium. In the FE analyses it was assumed that this difference was one order of magnitude.

In situ London Clay. The peak drained strength parameters (c'_{peak} and ϕ'_{peak}) of the London Clay foundation were derived from the laboratory test data presented in Fig. 8, whereas the drained residual strength parameters (c'_{res} and ϕ'_{res}) were adopted on the basis of the back-analysis of failures of cuttings made in London Clay (Potts *et al.*, 1997). The top few metres of the London Clay are weathered, and a drop in the strength from peak to residual was assumed, based on triaxial compression and ring shear tests, to occur between

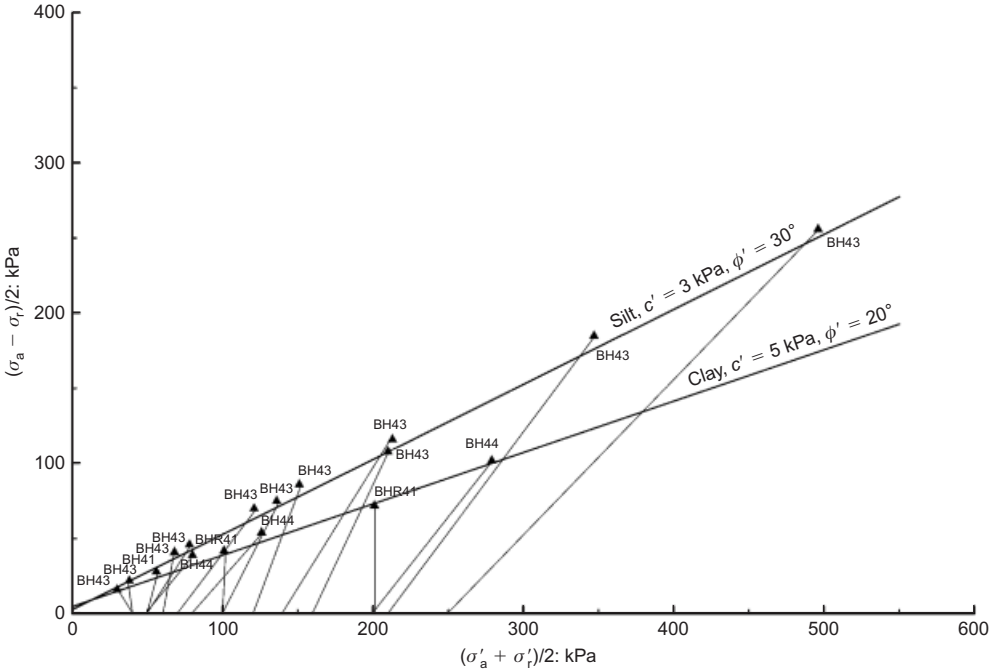

Fig. 7. Observed effective stress failure points in triaxial compression tests on isotropically consolidated samples of alluvium and adopted failure envelopes

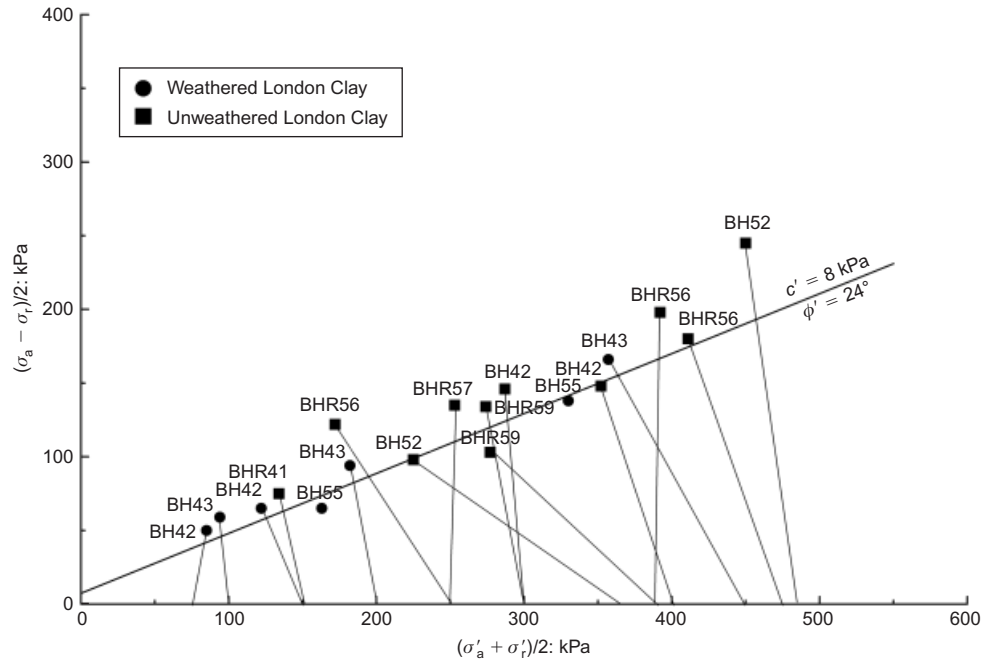

Fig. 8. Observed effective stress failure points in triaxial compression tests on isotropically consolidated samples of in situ London Clay and adopted failure envelope

shear strains $\varepsilon^{p}_{D,peak} = 5\%$ at peak and $\varepsilon^{p}_{D,res} = 20\%$ at residual (see Table 1). It is likely that the unweathered London Clay at depth will be stronger and consequently more brittle, but this has not been distinguished in the analyses.

The peak undrained shear strength, S_u, of the in situ London Clay can be deduced from the peak effective stress strength parameters (c'_{peak} and ϕ'_{peak}) and the mean effective stress in the ground, p'. The latter depends on the adopted bulk unit weight of the soil, γ, assumed pore water pressure distribution in the ground, and adopted profile of the coefficient of earth pressure at rest, K_0. However, it should be noted that in the Mohr–Coulomb model employed in the FE analyses the undrained shear strength also depends on the stress conditions operating in the ground (e.g. triaxial compression, plane strain and triaxial extension) and consequently can vary during the analysis, even without changes in the mean effective stress p' that occur during consolidation.

In Fig. 9 profiles of $(q_c - \sigma_{v0})$ have been superimposed for CPTs downstream of the dam toe. To provide a match with the results of the UU triaxial compression tests on U100 samples of the in situ London Clay, it has been necessary to apply an N_k factor of 20 to the cone data. This interpretation leads to an estimated undrained strength profile increasing from 35 kPa at a depth of 4 m to 90 kPa at 16 m.

The predicted plane-strain undrained shear strength profile in the London Clay foundation beyond the toe of the existing dam is also shown in Fig. 9, where it can be seen to tend towards a lower bound to the measured (or deduced) triaxial compression values.

The stiffness of the London Clay is non-linear and, for simplicity, was assumed to depend only on the mean effective stress p', and not on shear strain level. In the absence of adequate laboratory tests, the London Clay stiffness was selected on the basis of the assumed ratio between the undrained Young's modulus and undrained shear strength

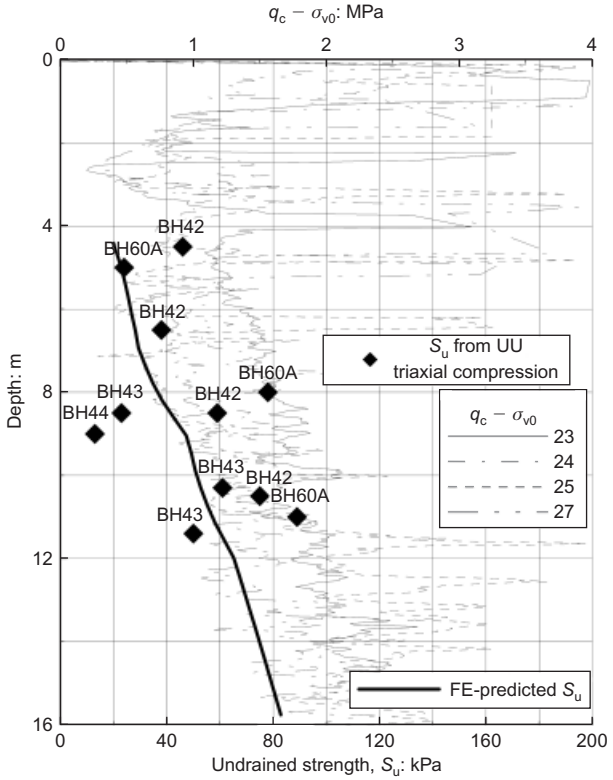

Fig. 9. Observed and predicted undrained strength in London Clay beyond downstream toe of existing embankment

$E_u/S_u = 200$, which is approximately valid for a typically predicted shear strain range between $\varepsilon^{p}_{D} = 0{\cdot}5\%$ and $1{\cdot}0\%$ in the London Clay foundation beneath the embankment.

The permeability of the London Clay reduces with depth, and is relatively low. In the analysis reported herein it was assumed to vary with the mean effective stress, p', according to an exponential function (see Table 1), reasonably matching available permeability data for the east of the London Clay basin (see Hight *et al.*, 2003).

FINITE-ELEMENT ANALYSES

The typical cross-section of the existing dam shown in Fig. 2 was selected for the FE analyses. The FE mesh is shown in Fig. 10(a). The same mesh has been used for the analyses of both the original dam failure (note that the original dam is marked by the shaded areas in Figs 10(a) and 10(b)) and the subsequently reconstructed embankment. It should be noted that the actual dam geometry and embankment's zoning were simplified for the purpose of analysis, as shown in Fig. 10(b). For example, the presence of a gravel-filled vertical wall drain within the existing downstream shoulder (see Fig. 2) was omitted, because its impact on the results was considered to be negligible. Similarly, the various drainage blankets and/or granular filters were not directly modelled in the analyses; their action was taken into account by imposing appropriate 'zero' pore water pressure boundary conditions during various stages of the analysis.

The FE analyses modelled both the short- and long-term behaviour of the embankment and its foundation. Apart from the granular materials used in construction of the main embankment, which were assumed to behave in a drained manner, the permeability of all other materials was specified. Even in the short term, the behaviour of these materials was partially drained according to the permeabilities and time steps specified in the 'coupled' FE analyses.

The FE analyses were performed in two dimensions using a plane-strain approach. Eight-noded iso-parametric FE elements with 'reduced' 2×2 integration order were used. All eight nodes of an element had displacement degrees of freedom, whereas the pore water pressure degrees of freedom of 'consolidating' elements were specified only at the four corner nodes. A modified Newton–Raphson approach with a sub-stepping stress point algorithm was used to solve the FE equations (Potts & Zdravkovic, 1999).

No horizontal displacements were allowed on the vertical boundaries of the embankment foundation, whereas the bottom foundation boundary was fixed in both the vertical and horizontal directions. In the coupled FE analyses, the bottom and vertical boundaries of the foundation and the surface (top) boundary of each embankment clay layer during construction were assumed to be impermeable. However, the interface between the clay and the drained granular fill in the embankment was modelled as permeable, always assuming the granular fill to be a source of water during both construction and subsequent impounding and reservoir operation, by specifying appropriate values of the pore water pressures.

The best estimate of the history of dam construction and operation was modelled in the analysis, as outlined in Table 2, which shows the increment numbers corresponding to the various stages of the analyses and appropriate time steps. The methods used for modelling excavation, fill construction and reservoir impounding are described by Potts & Zdravkovic (2001).

Monitoring of convergence in the analyses involving strain-softening, and consequently progressive failure, is not easy. There is also a potential influence of the thickness of

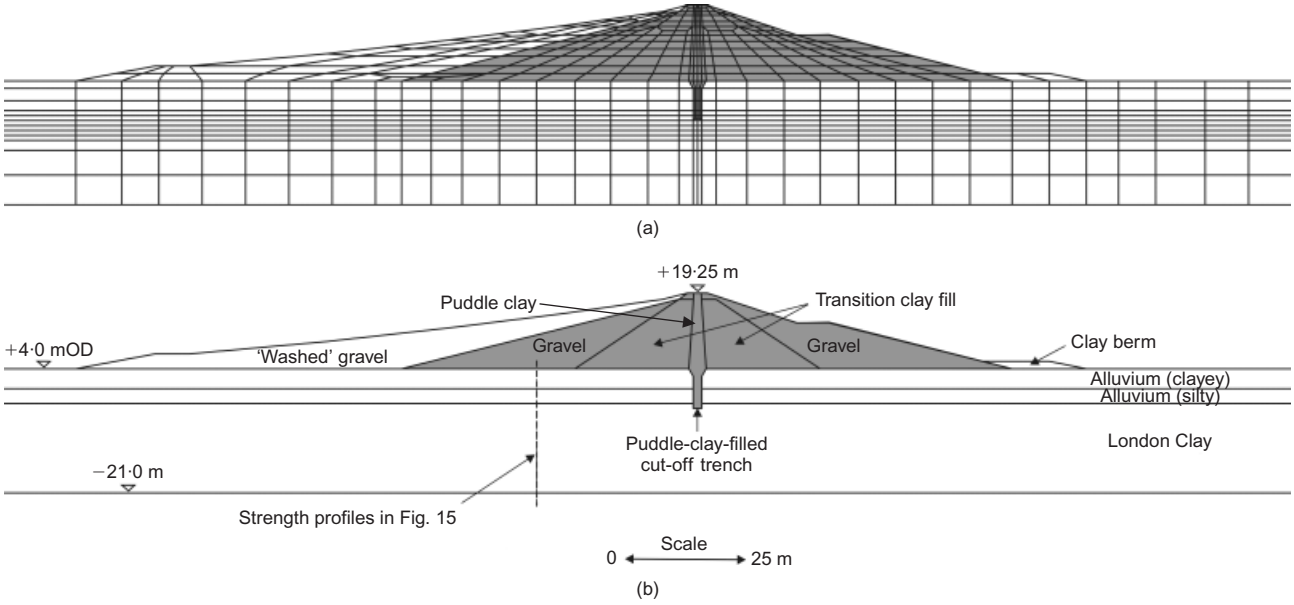

Fig. 10. (a) Finite-element mesh and (b) zoning of existing embankment

finite elements on the results from such numerical analyses. To overcome these difficulties, the same approach as applied in earlier papers (see e.g. Potts *et al.*, 1990, 1997) was used herewith.

RESULTS OF THE ANALYSES

The results are related to (a) the failure during construction of the original dam, and (b) construction and subsequent operation of the reconstructed dam. They are referred to the increment numbers according to the modelled construction sequence as presented in Table 2.

Failure of the original dam

French *et al.* (2000) reported that the fill for the original embankment (marked by the shaded areas in Figs 10(a) and 10(b)) had been raised in 11 months, although it is not clear whether this time period covered any cut-off trench filling. In the FE analysis a uniform filling rate was assumed, although it is likely that the rate of filling speeded up as the embankment was reaching its full height.

Figure 11 shows the results of the FE analysis for increment 19 when the level of filling reached El. +17·25 mOD and the embankment is still stable. There is a build-up of pore water pressures in the materials of low permeability, such as the London Clay in the foundation and the clay embankment fill (Fig. 11(a)). For the latter this is despite the negative pore water pressures (suctions) prescribed in the 'newly' constructed elements (see the section 'Model parameters' above). It is important to note that there is also a build-up of pore water pressures in the alluvium next to the cut-off trench and beneath the transition clay fills. However, it appears that the gravel used in dam construction and the more permeable silty alluvium in the foundation successfully drain the alluvial clay beneath the outer parts of the embankment shoulders.

The maximum predicted movement vector for this stage of filling is 0·33 m, and is mostly a consequence of undrained shearing in the London Clay foundation (Fig. 11(b)). Fig. 11(c) shows the contours of shear stress level. The shaded areas inside the contour 1·0 indicate that the shear strength is fully mobilised in the top of the in situ London Clay and a large part of the alluvium.

The analysis predicted the failure of the upstream shoulder during placement of the layer of fill between El. +17·25 m and +18·0 mOD (approximately 2 m from the intended top of the embankment at +19·5 mOD). To capture the onset of

Table 2. Modelled construction sequence

Increment number	Description of event	Time
0	Set up initial stresses	–
1–6	Cut-off trench excavation	4·5 months
7–10	Cut-off trench filling	4·5 months
11–23	Original embankment filling to El. +18·0 mOD	7·2 months
24–30	Removal of fill above +9·0 mOD after failure	2·52 months
31–41	Filling for reconstructed embankment to El. +19·25 mOD	6·6 months
42–45	Dissipation	12 months
46–50	First reservoir impounding to TWL (El. +17·8 mOD)	21 months
51	Reservoir drawdown to El. +16·25 mOD	6 months
52, 53	Dissipation of excess pore water pressure (during Second World War) with reservoir level at El. +16·25 mOD	5·75 years
54	Reservoir re-impounding to TWL (El. +17·8 mOD)	6 months
55–60	Dissipation of excess pore water pressure at TWL (El. +17·8 mOD)	50 years

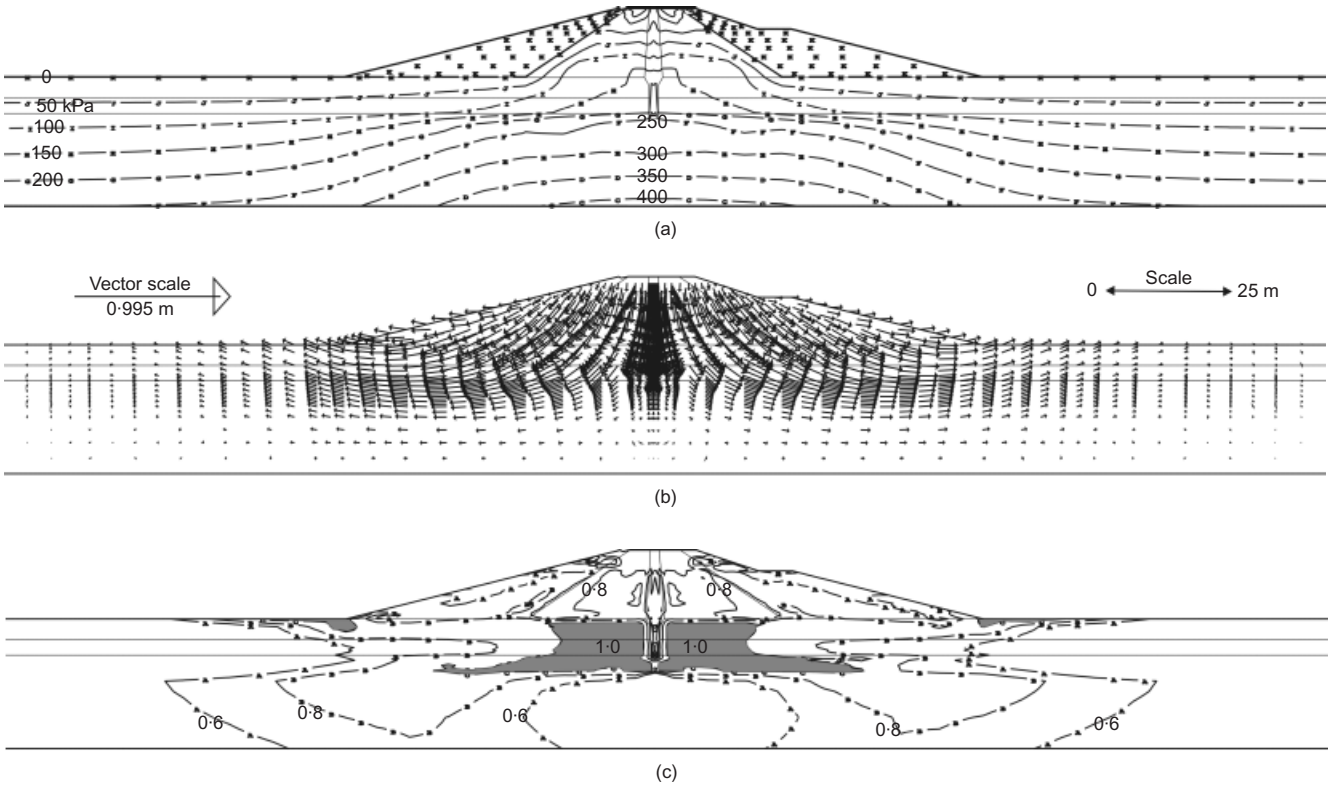

Fig. 11. Construction of original dam when it reached El. +17·25 mOD (increment 19): (a) contours of pore water pressure; (b) accumulated movement vectors since filling of cut-off trench (note that maximum predicted movement vector is always a third of quoted number – and vector length – in vector scale shown); (c) contours of stress level

the embankment failure more precisely, the last 0·75 m thick layer of fill was placed over four increments (increments 20 to 23), prescribing a short time step equivalent to 0·001 year (0·365 days) for each increment.

The results are presented for the last three increments (increments 21 to 23) in terms of the incremental movement vectors (Fig. 12) and contours of the plastic shear strain invariant, ε_D^p (Fig. 13), as defined in Table 1 and the

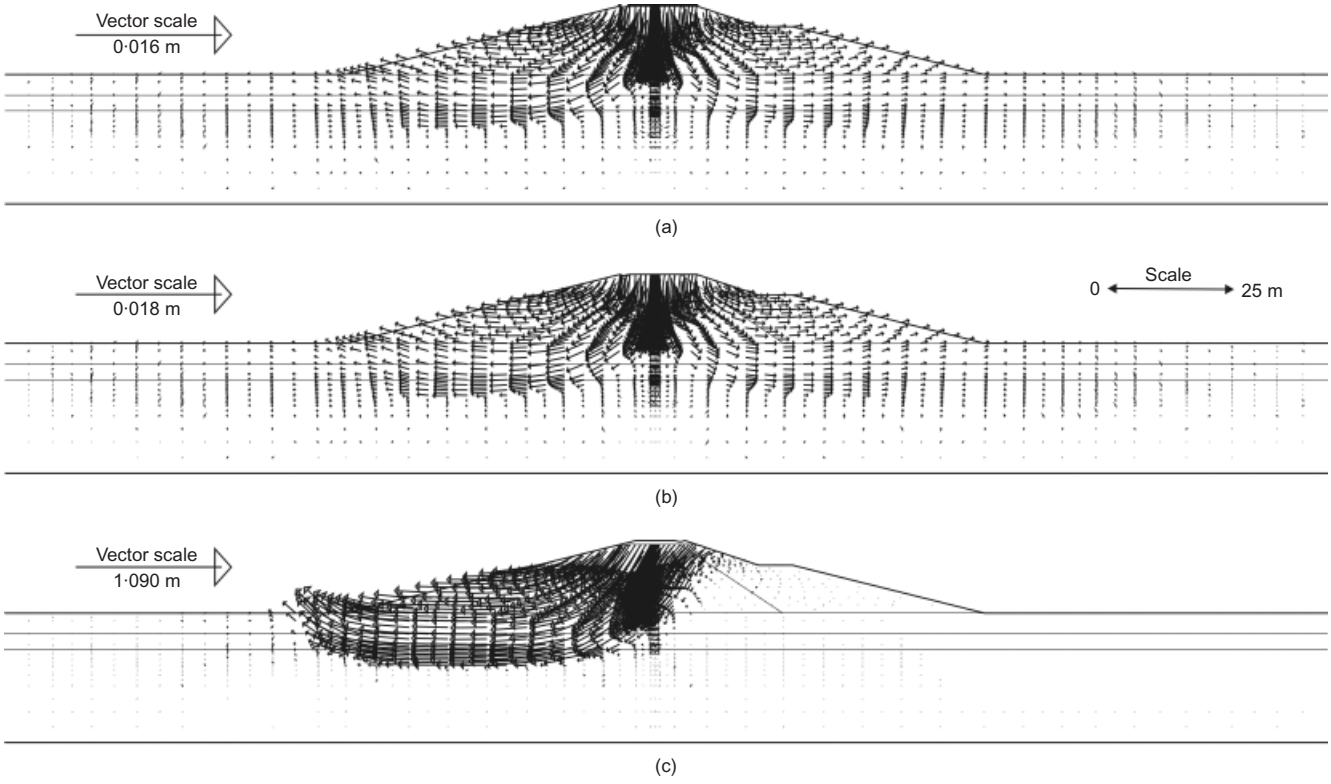

Fig. 12. Incremental movements vectors just prior to and during failure of original dam: (a) increment 21; (b) increment 22; (c) increment 23

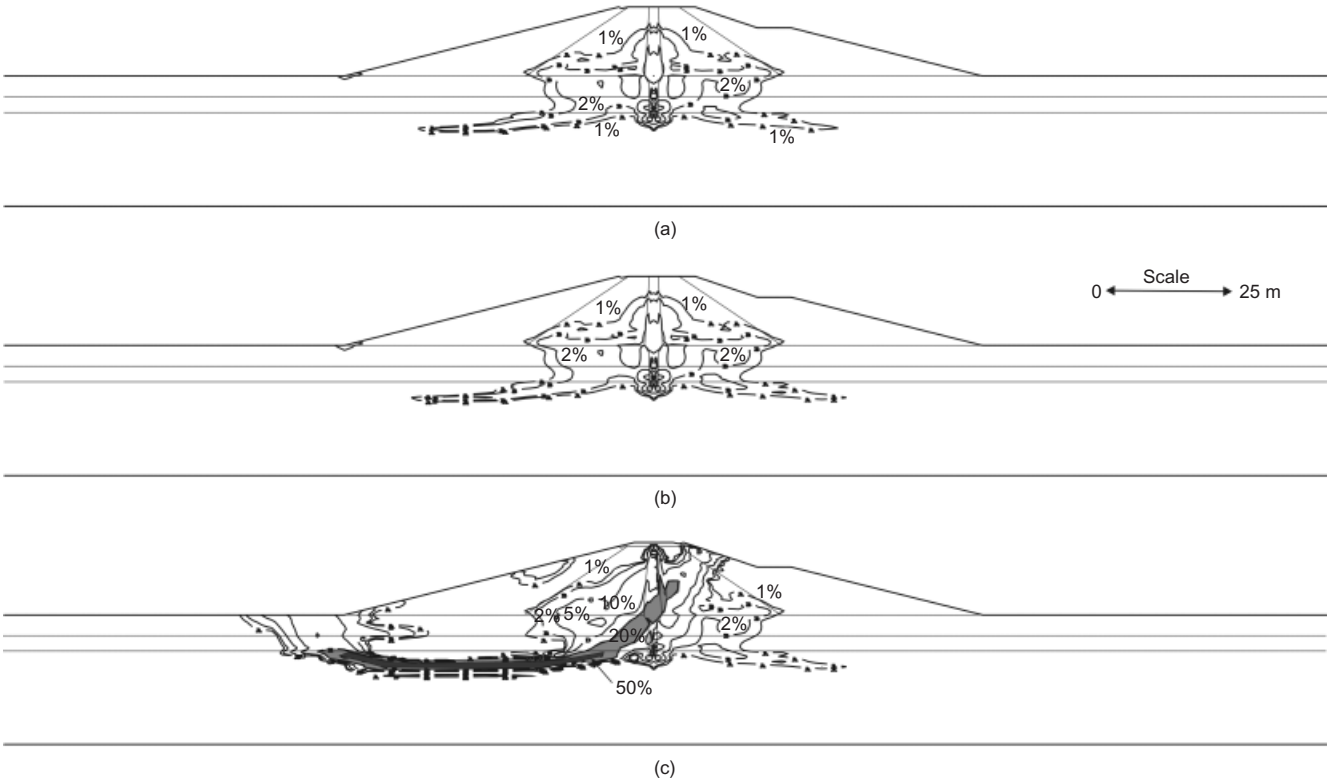

Fig. 13. Contours of accumulated plastic shear strain invariant just prior to and during failure of original dam: (a) increment 21; (b) increment 22; (c) increment 23

Appendix. For the London Clay these contours give information about the mechanism of progressive failure.

The clear progression towards failure can be easily seen. The failure is sudden, and took place in the last increment of filling (increment 23), which corresponds to the placement of $(18{\cdot}0 - 17{\cdot}25)/4 = 0{\cdot}1875$ m of fill, equivalent to a pressure of 3·6 kPa. Large movements (in excess of 1 m) are predicted during the collapse (Fig. 12(c)), although the particular increment of the analysis (increment 23) did not converge, because the stress equilibrium conditions were not satisfied any longer. In the field, equilibrium was reached only after horizontal outward movements of more than 15 m and crest settlement of 3–3·5 m (see Fig. 4), emphasising the brittleness of the collapse, and showing that failure did not occur on pre-existing shear surfaces. These post-collapse movements were not modelled in the analyses. However, in the analyses large shear strains, in excess of $\varepsilon_D^p = 50\%$, were predicted in the top of the London Clay foundation (Fig. 13(c)), so that there is no doubt that a low residual shear strength operates in the London Clay foundation, even after predicted movements of just 1 m.

Development of the horizontal movement of both the upstream and downstream slopes of the original embankment at El. +9·0 mOD due to placement of the fill above is shown in Fig. 14. The behaviour of the upstream and downstream slopes is similar until the level of the berm at the downstream slope (El. +13·25 mOD) is reached. A small, but beneficial, effect of the berm in reducing the downstream slope horizontal movements can be seen. The analysis therefore suggests that the presence of the downstream berm is the main reason why the upstream slope collapsed in advance of the downstream one, although local variations in the field (which are not modelled in the analysis) could also be a contributing factor. Fig. 14 also confirms that the predicted failure of the upstream slope takes place suddenly with no warning, at least as far as the predicted movements are concerned.

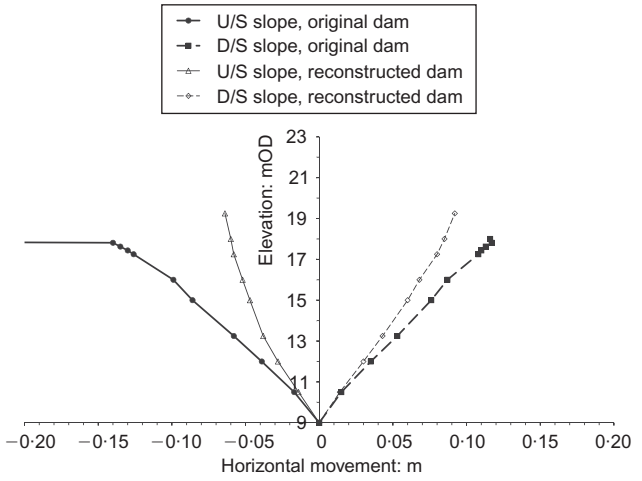

Fig. 14. Predicted horizontal movement of upstream and downstream slopes at El. +9·0 mOD during construction of original and existing dam

Figure 15 shows the predicted undrained (plane strain) shear strength profiles in the foundation during construction of the original embankment 32·5 m upstream from the dam centreline. There is an increase in the shear strength of the alluvium, because it partially consolidates during construction. The increase is higher in the lower, silty alluvium than in the upper, clayey layer because of its higher permeability. Perhaps surprisingly, a reasonable amount of consolidation is also predicted to take place in the top 2 m of the London Clay underlying the more permeable silty alluvium, so that the rupture surface through the London Clay is pushed further down (3 m from the top of the London Clay) where the London Clay is less strong because of an apparent lack of consolidation.

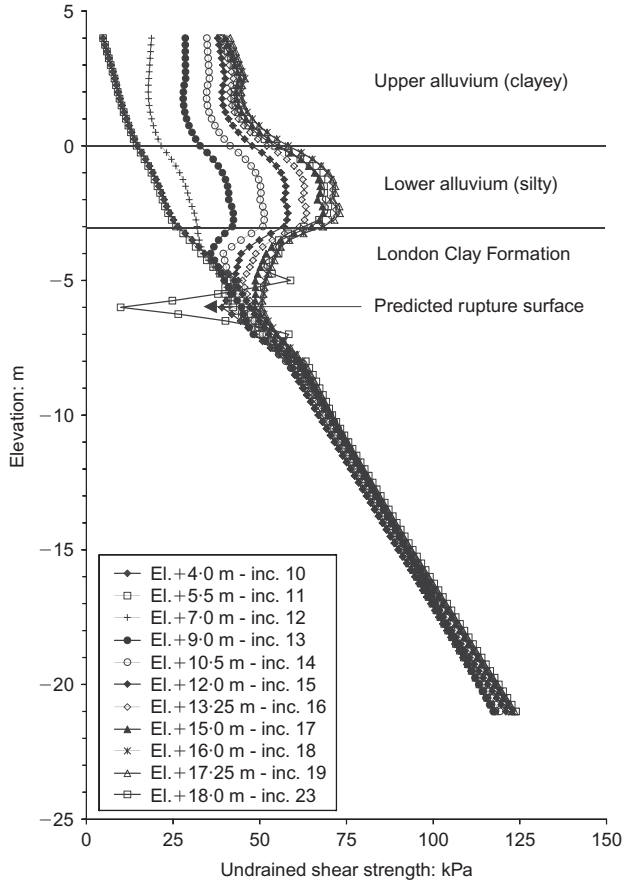

Fig. 15. Predicted profiles of undrained shear strength in foundation during construction of original dam 32·5 m upstream from dam centreline

The FE analysis of the original dam succeeded in predicting the failure towards the end of its construction (i.e. 1·6875 m short of the embankment's full height of 15·5 m, compared with the observed 2 m). It confirmed a rather deep-seated failure mechanism postulated by French *et al.* (2000), which involved shearing through the top of the London Clay foundation rather than a non-circular failure mechanism through the alluvium, as advocated by Watson Hawksley (1990) (see also Fig. 3). However, the predicted rupture surface appeared to be somewhat deeper (3 m below the top of the London Clay) than expected, because the top 2 m of the London Clay gained strength owing to its consolidation into the overlying more permeable alluvium. This was in spite of the rapid embankment filling that was modelled in the analysis.

Existing dam

After the simulated failure of the original embankment, the analysis modelled the removal of the fill material to El. +9·0 mOD, as shown approximately in Fig. 3 (increments 24 to 30; see Table 2). There is some uncertainty as to what in reality had been removed before the reconstructed embankment was built. For simplicity, the FE analysis modelled the removal of the fill material above El. +9·0 mOD in layers without leaving any of the 'unfailed' fill material in the downstream embankment shoulder.

Reconstruction of the embankment started with placement of a small clay berm at the downstream toe (see Fig. 10(b), increment 31). The granular fill constituting the washed gravel was then placed in front of the general gravel, which had not previously been removed, forming a substantially flatter upstream slope than was achieved during construction of the original embankment. When the filling reached El. +9·0 mOD (increment 34), both granular and clay fill started being placed in horizontal layers across the whole embankment width until the crest level of the reconstructed dam reached El. +19·25 mOD (increment 41).

The results for this stage of the analysis are shown in Figs 16 and 17. The pore water pressures (Fig. 14(a)) increased again in the London Clay foundation, this time more below the upstream shoulder than the downstream one, reflecting the fact that more fill material is being placed into the upstream shoulder in order to form a flatter slope. The maximum predicted settlement during reconstruction is 0·27 m (Fig. 16(b)). The shear strength is mobilised in the foundation below the inner part of the upstream shoulder – that is, below the transition clay fill, in the alluvium and along the existing rupture surface formed in the top of the London Clay foundation during the failure of the original embankment where the residual strength still operates (Fig. 16(c)). However, it appears that the additional granular fill in the form of the washed gravel provides adequate stability of the reconstructed upstream slope. There is no concentration of the incremental movement vectors (Fig. 17(a)) or signs that the existing rupture surface in the London Clay is extended (compare Figs 13(c) and 17(b)) by the reconstruction of the embankment.

The downstream slope is also stable, although the shear strength is mobilised in the clayey alluvium just behind the puddle-clay-filled cut-off trench (Fig. 16(c)). The predicted plastic shear strains have not increased, and the maximum values below the downstream shoulder are still around $\varepsilon_D^p = 2\%$ (compare Fig. 17(b) with Fig. 13(c)). This is not surprising, given that the foundation beneath the downstream embankment slope could only have gained in strength since the failure of the upstream slope of the original dam.

The predicted horizontal movements of the 'same' downstream and 'new' flatter upstream slopes at El. +9·0 mOD during reconstruction are also shown in Fig. 14. Clearly, their magnitude is now smaller, and more importantly, the rate of the horizontal movements appears to reduce as the fill at higher elevations is placed, indicating the improved stability of the reconstructed embankment in comparison with the original one.

The reconstructed dam was impounded to the intended TWL at El. +17·8 mOD over a period of 33 months (increments 42 to 50) since the end of its construction in August 1938. By the end of impounding there is further consolidation of the foundation beneath the downstream shoulder (Fig. 18(a)) and consequently an increase in undrained strength (Fig. 19). It seems that during a period of 33 months the alluvium consolidated fully under the weight of the downstream embankment shoulder. However, a longer period of time is needed for the full consolidation (and full gain in strength) of the less permeable in situ London Clay.

During the Second World War the reservoir level was lowered to approx. El. +16·25 mOD for safety reasons (increments 51 to 53), before it was raised again to the intended TWL at El. +17·8 mOD (increment 54) in March 1947. The analysis then modelled dissipation of the excess pore water pressures, keeping the reservoir full until the present time (increment 60).

The analysis indicates that the steady-state pore water pressures with the reservoir full at El. +17·8 mOD were reached well before the present time. They are shown in Fig. 18(b). The predicted seepage pressures, expressed as the pore water pressure head (in metres) across the puddle-filled cut-of trench at El. −1·0 mOD and the puddle clay core at El. +8·0 mOD are shown in Fig. 20. The measured pore water pressures (head) from two piezometers installed just 3 m and 6 m downstream from the dam centreline (French *et*

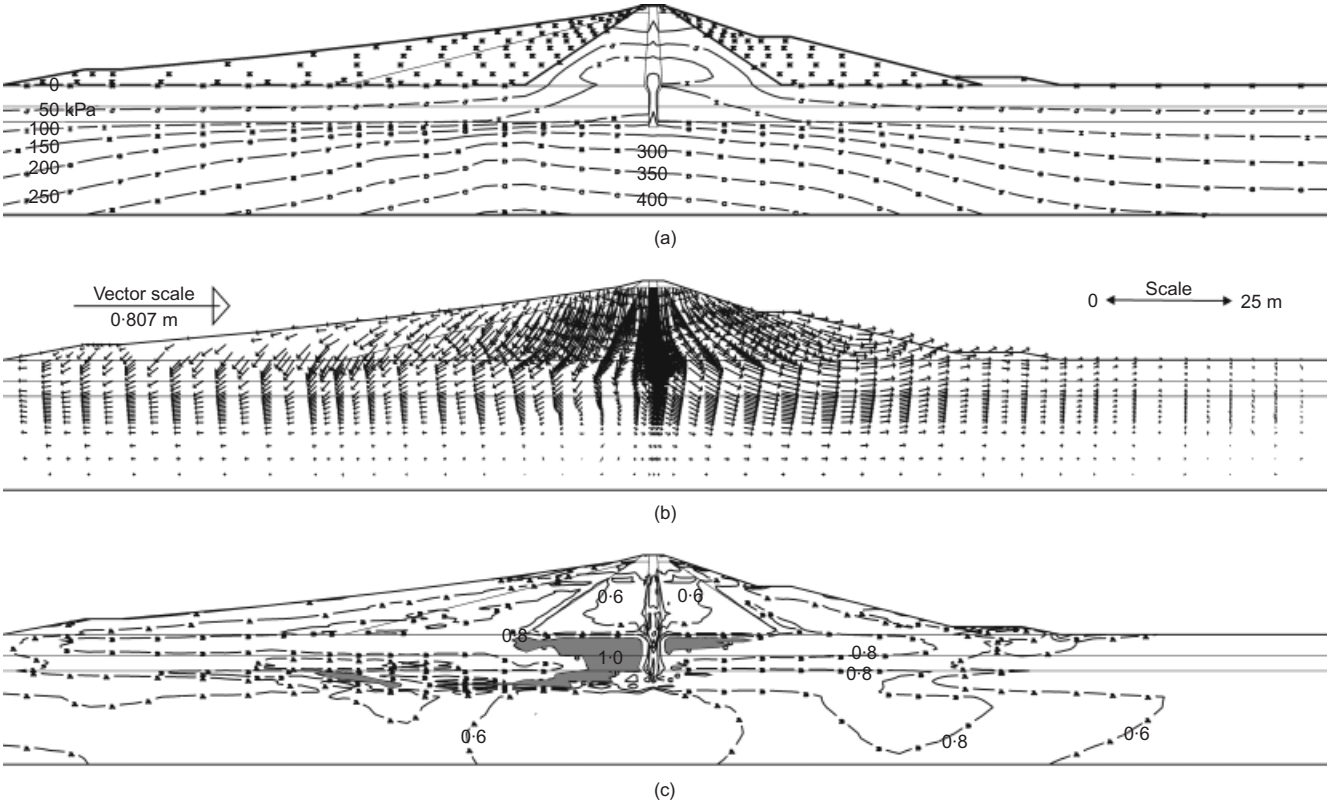

Fig. 16. Construction of existing dam when it reached the crest El. +19·25 mOD (increment 41): (a) contours of pore water pressure; (b) accumulated movement vectors during construction of reconstructed embankment; (c) contours of stress level

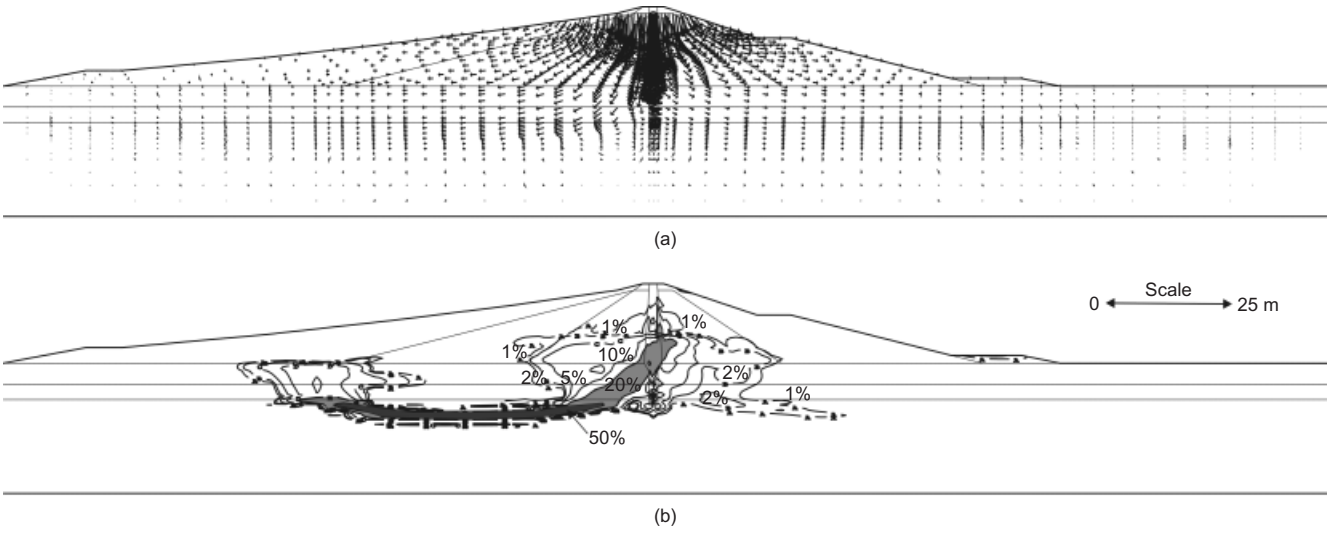

Fig. 17. (a) Predicted incremental movement vectors and (b) contours of accumulated plastic shear strain invariant at the time of construction of existing dam (increment 41)

al., 2000) are also indicated. The matching achieved by the analysis is excellent.

The predicted settlement profiles through the clay core, cut-off trench and London Clay beneath are shown in Fig. 21, indicating the maximum long-term crest settlement (increments 42 to 60) to be 0·193 m. However, the predicted crest settlement since the first full reservoir impounding (increments 51 to 60) is less than 0·1 m, suggesting that a significant amount of the dam settlement (more than 0·1 m) took place during the first reservoir impounding over a relatively short time period of 33 months (increments 42 to 50), owing to dissipation of the excess pore water pressures built up in the puddle clay core (and clay transition fill) during the dam construction. It should be noted that the long-term dam settlements observed since the end of construction are now in excess of 0·6 m (Watson Hawksley, 1990). The apparent difference can be explained by creep and reservoir operation settlements (see e.g. Tedd *et al.*, 1997; Vaughan *et al.*, 2004), which the current analysis does not account for.

The construction-induced excess pore water pressures in the foundation have dissipated over more than 70 years since the existing embankment was constructed, and the alluvium and London Clay in the foundation are now substantially stronger than they were before the dam construction (see Fig. 19). Consequently, the stability of the reconstructed embankment at present is significantly enhanced.

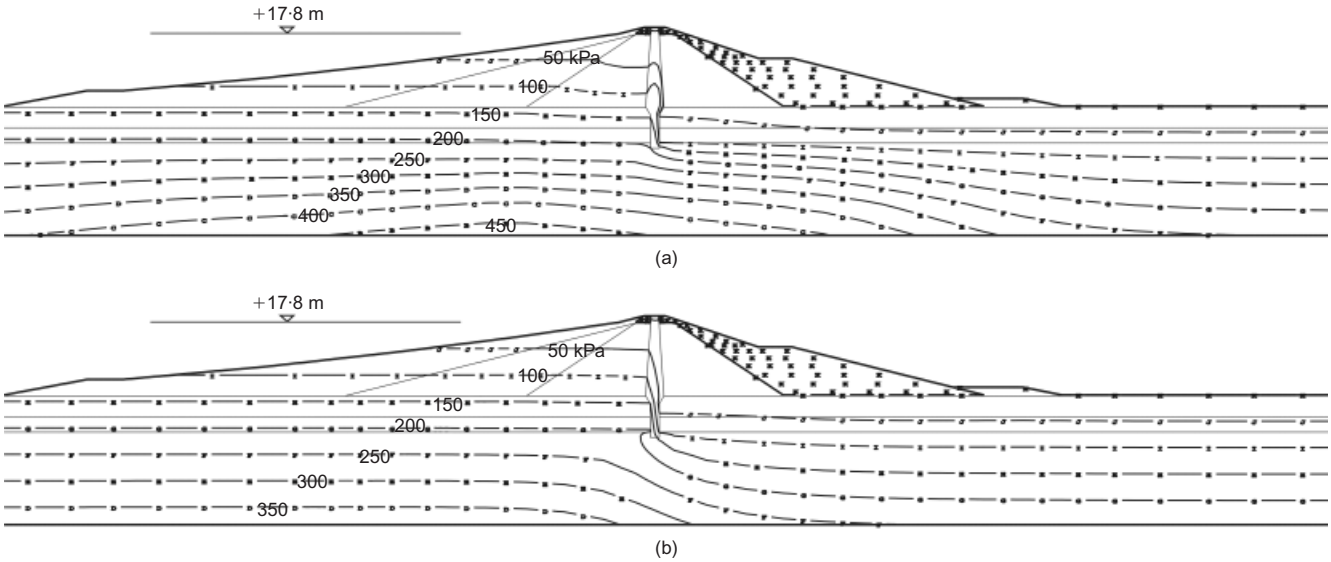

Fig. 18. Predicted contours of pore water pressure: (a) at end of impounding of existing dam (increment 50); (b) in the long term with reservoir full (increment 60)

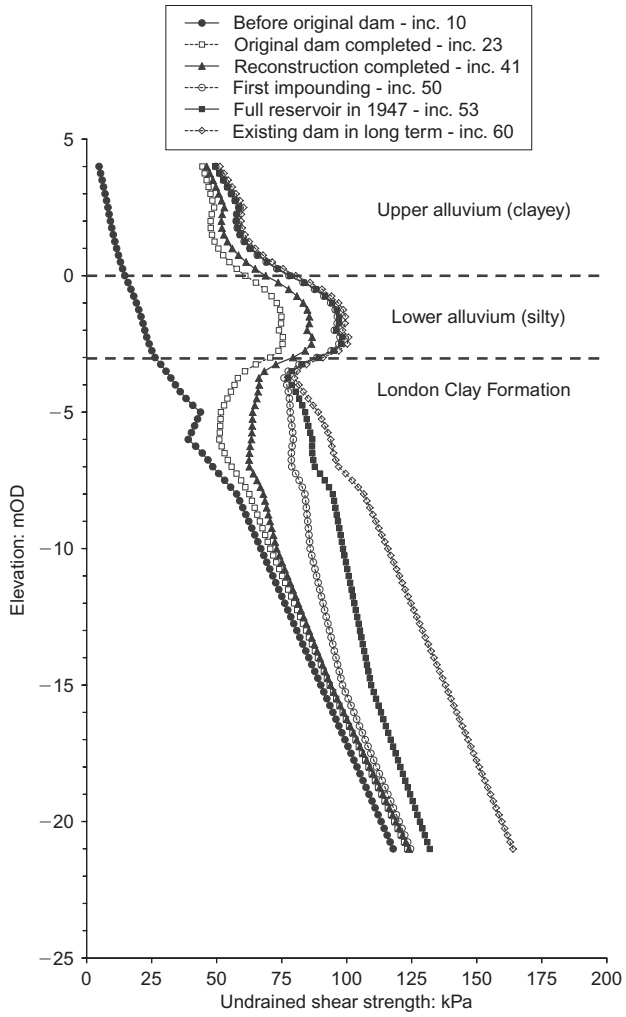

Fig. 19. Predicted profiles of undrained shear strength in existing dam foundation 32·5 m downstream from dam centreline

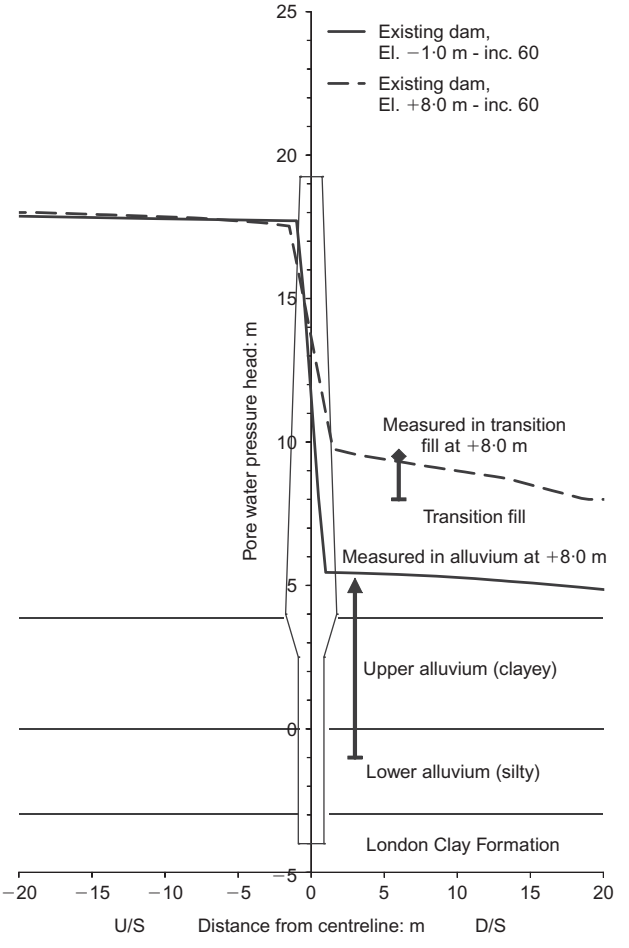

Fig. 20. Predicted and measured pore water pressure head of existing dam in the long term

CONCLUSIONS

Advanced FE analyses were carried out to investigate both the failure towards the end of construction of the original dam at Abberton and the stability of the main existing embankment. Appropriate constitutive models to characterise the observed behaviour of the various materials involved were chosen, and the model parameters were derived on the basis of the available site investigations and laboratory testing, and previous experience.

The analyses successfully predicted the upstream slope failure of the original embankment in July 1937. The embankment failed through the mechanism of progressive

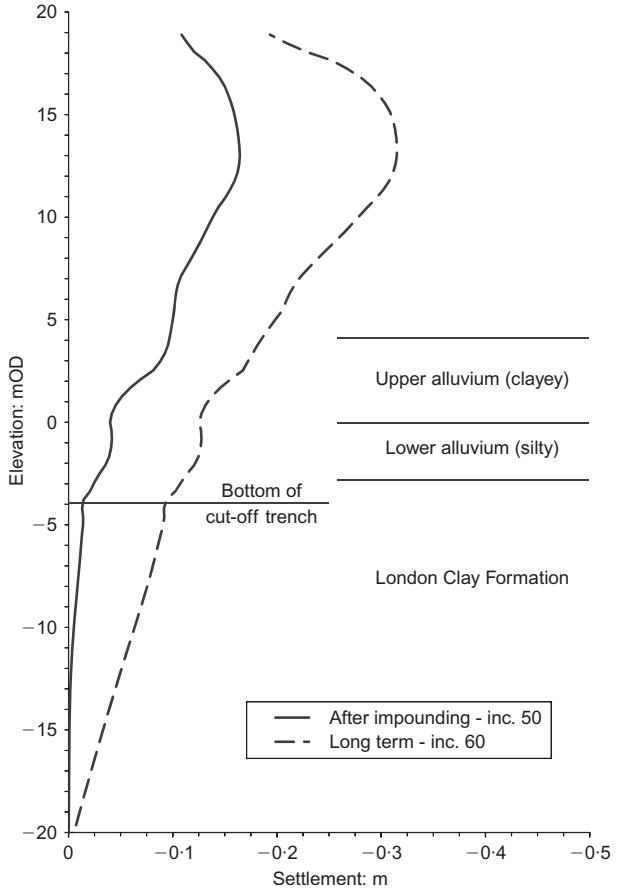

Fig. 21. Predicted settlement profiles along centreline of existing dam

failure involving the top of the stiff plastic London Clay, which had not consolidated under the weight of the embankment (Fig. 22(a)). It is interesting to note that the embankment at Chingford also failed through the mechanism of progressive failure, but the failure was not deep-seated as at Abberton, instead involving a superficial 1 m thick partially consolidated layer of yellow alluvial clay overlying the river gravel deposits (Fig. 22(b)). However, the mechanism of progressive failure at the two embankments was different: at Abberton the softening of the London Clay started in the central portion of the dam propagating outside (see Fig. 13), whereas at Chingford the softening was instigated near the embankment toe and extended towards the core (Dounias *et al.*, 1988).

It should be emphasised that both the failed dams at Abberton and Chingford were designed according to traditional methods that had been successfully used in the past. The various fill materials used in the dams' construction were not compacted, but were spread using modern earth-moving equipment, a novelty at the time. Construction was therefore faster than previously adopted, reducing the time available for pore water pressures to dissipate during construction. The relatively rapid rate of embankment filling achieved by using modern earth-moving equipment can be considered to be a major contributing factor to both dams' failures.

The analyses at Abberton also modelled the dam reconstruction, which adopted a flatter upstream slope, and its first reservoir filling and subsequent operation. The analyses predicted satisfactory behaviour of the existing dam, and its response was similar to that observed. Thus the constitutive models used and the parameters derived were successfully calibrated against the observed behaviour of both the original and existing main dams at Abberton, and could be used with some confidence in the analyses of main dam raising.

APPENDIX: GENERALISED MOHR–COULOMB MODEL

A generalised non-linear elastic strain-softening/hardening plastic model incorporating a Mohr–Coulomb yield criterion given by the apparent cohesion, c', the angle of shearing resistance, φ', and the angle of dilation, ψ, is used.

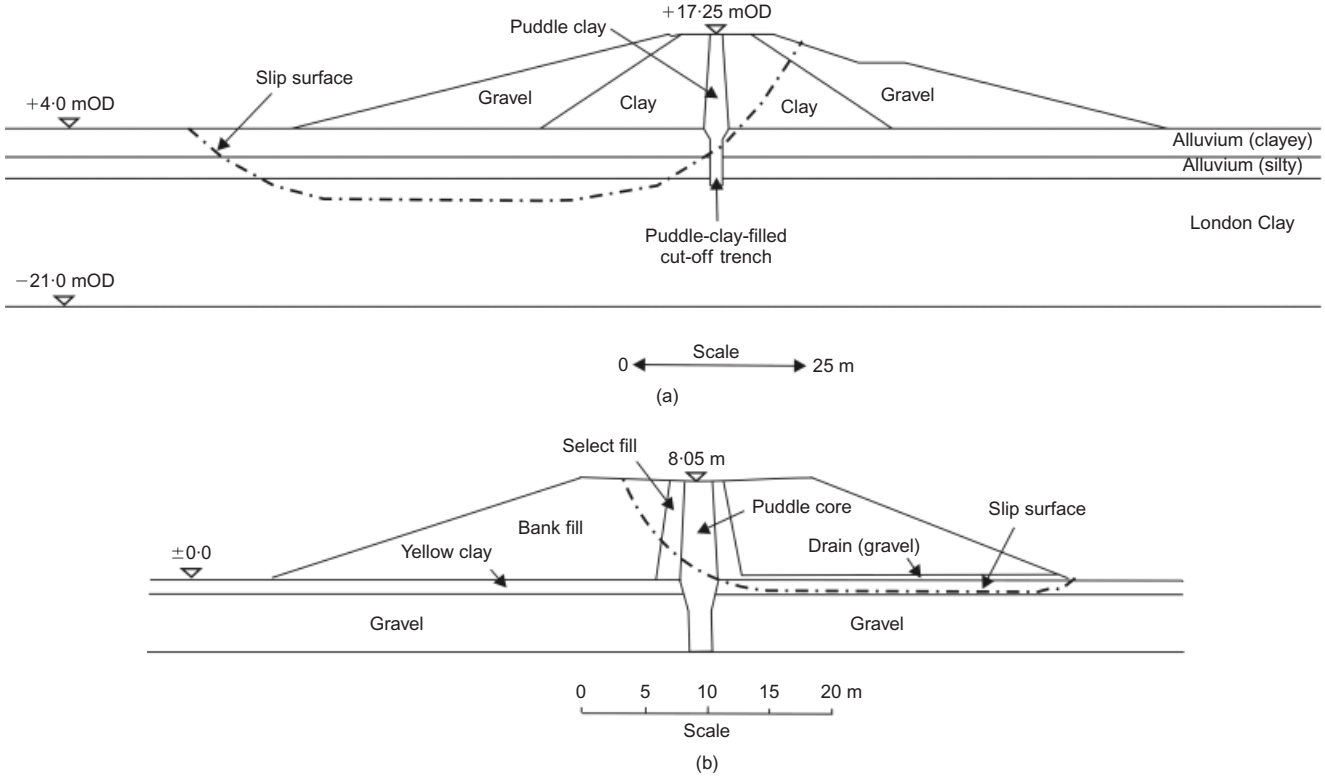

Fig. 22. Idealised dam geometries and predicted failures at: (a) Abberton; (b) Chingford (after Dounias *et al.*, 1988)

The Young's modulus, E, varies according to the mean effective stress, p'

$$E = ap' \tag{1a}$$

or

$$E = b\left(\frac{p' + 100}{100}\right) \tag{1b}$$

where a and b are dimensionless parameters, and the Poisson's ratio, μ, is constant.

The yield function is given by

$$F(\sigma') = S - 1 \tag{2}$$

and S is the shear stress level, defined as

$$S = \frac{J}{(p' + \alpha)g(\theta)} \tag{3}$$

where

$$p' = \frac{\sigma'_1 + \sigma'_2 + \sigma'_3}{3} \tag{4}$$

$$J^2 = \frac{(\sigma'_1 - \sigma'_2)^2 + (\sigma'_2 - \sigma'_3)^2 + (\sigma'_3 - \sigma'_1)^2}{6} \tag{5}$$

$$g(\theta) = \frac{\sin\phi'}{\cos\theta + (\sin\theta \sin\phi'/\sqrt{3})} \tag{6}$$

$$\theta = \tan^{-1}\left(\frac{2b - 1}{\sqrt{3}}\right) \tag{7}$$

$$b = \frac{\sigma'_2 - \sigma'_3}{\sigma'_1 - \sigma'_3} \tag{8}$$

α is the intercept of the yield surface on the mean effective stress (p') axis and is given by

$$\alpha = \frac{c'}{g(\theta = 0)} = \frac{c'}{\sin\phi'} \tag{9}$$

where c' is the cohesion intercept with Lode angle $\theta = 0$: that is, $\sigma'_2 = (\sigma'_1 + \sigma'_3)/2$.

The plastic potential is defined in the same way as the yield function, but with the angle of shearing resistance, ϕ', replaced by the angle of dilation, ψ.

Softening behaviour of the in situ London Clay is introduced by allowing the angle of shearing resistance, ϕ', and the cohesion intercept, c', to vary with the deviatoric plastic strain invariant $\varepsilon^{\mathrm{p}}_{\mathrm{D}}$ (see Fig. 23), defined as

$$\left(\varepsilon^{\mathrm{p}}_{\mathrm{D}}\right)^2 = \frac{2}{3}\left[\left(\varepsilon^{\mathrm{p}}_1 - \varepsilon^{\mathrm{p}}_2\right)^2 + \left(\varepsilon^{\mathrm{p}}_2 - \varepsilon^{\mathrm{p}}_3\right)^2 + \left(\varepsilon^{\mathrm{p}}_3 - \varepsilon^{\mathrm{p}}_1\right)^2\right] \tag{10}$$

The angle of dilation, ψ, may also be varied with $\varepsilon^{\mathrm{p}}_{\mathrm{D}}$. Such softening is modelled only for the in situ London Clay in the foundation. Other materials are assumed to behave in a perfectly plastic manner.

The model parameters are listed in Table 1.

In non-dilative soils ($\psi = 0$), the undrained shear strength, S_{u}, predicted by the model is given by

$$S_{\mathrm{u}} = \frac{J\cos\theta}{(p' + \alpha)g(\theta)} \tag{11}$$

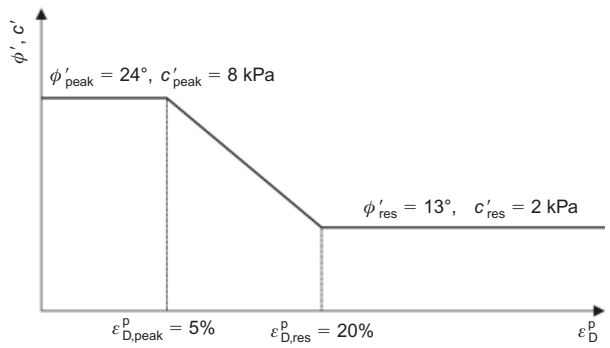

Fig. 23. Variation of angle of shearing resistance, ϕ', and cohesion intercept, c', with deviatoric plastic strain invariant, $\varepsilon^{\mathrm{p}}_{\mathrm{D}}$

This expression reduces to

$$S_{\mathrm{u}} = \left(\frac{c'\cos\phi'}{\sin\phi'} + p'_i\right)\sin\phi' \tag{12}$$

and

$$S_{\mathrm{u}} = \left(\frac{c'\cos\phi'}{\sin\phi'} + p'_i\right)\sin\phi' \Big/ \left(1 - \frac{\sin\phi'}{3}\right) \tag{13}$$

for plane strain and triaxial (compression) conditions respectively, where p'_i is the current mean effective stress.

NOTATION

a, b	dimensionless parameters
c'	effective cohesion
c'_{peak}	peak cohesion
c'_{res}	residual cohesion
E_{u}	undrained Young's modulus
e	void ratio
K_0	coefficient of earth pressure at rest
k	coefficient of permeability
N	SPT blow count
N_{k}	cone factor
p'	mean effective stress
p'_i	current mean effective stress
q_{c}	cone resistance
S	suction; shear stress level
S_{u}	undrained shear strength
υ	specific volume
γ	bulk unit weight of soil
$\varepsilon^{\mathrm{p}}_{\mathrm{D}}$	deviatoric plastic strain invariant
$\varepsilon^{\mathrm{p}}_{\mathrm{D,peak}}$	deviatoric plastic strain invariant at peak
$\varepsilon^{\mathrm{p}}_{\mathrm{D,res}}$	deviatoric plastic strain invariant at residual
$\varepsilon^{\mathrm{p}}_1$, $\varepsilon^{\mathrm{p}}_2$, $\varepsilon^{\mathrm{p}}_3$	principal plastic strains
μ	Poisson's ratio
σ'	normal effective stress
σ'_{a}	axial effective stress
σ'_{r}	radial effective sress
σ_{v0}	full overburden stress
ϕ'	effective angle of shearing resistance
ϕ'_{crit}	critical state angle of shearing resistance
ϕ'_{peak}	peak angle of shearing resistance
ϕ'_{res}	residual angle of shearing resistance
ψ	angle of dilation

REFERENCES

Burland, J. B., Simpson, B. & St John, H. D. (1979). Movements around excavations in London Clay. *Proc. 7th Eur. Conf. Soil Mech. Found. Engng, Brighton* **1**, 13–29.

Clayton, C. R. I. (1995). *The standard penetration test (SPT): Methods and use*, CIRIA Report 143. London, UK: Construction Industry Research and Information Association.

Cooling, L. F. & Golder, H. Q. (1942). The analysis of the failure of an earth dam during construction. *J. Instn Civ. Engrs, London* **9**, No. 1, 38–55.

Dounias, G. T., Potts, D. M. & Vaughan, P. R. (1988). Finite element analysis of progressive failure: two case studies. *Comput. Geotechnics* **6**, No. 2, 155–175.

French, D. J., Woolgar, M. J. & Saynor, P. (2000). Geotechnical investigations at Abberton Dam, Essex. In *Dams 2000* (ed. P. Tedd), pp. 345–359. London, UK: Thomas Telford.

GCG (2009). *Abberton reservior: soil parameter selection – final report*. London, UK: Geotechnical Consulting Group.

Hight, D. W., McMillan, F., Powell, J. J. M, Jardine, R. J. & Allenou, C P. (2003). Some characteristics of London Clay. *Proceedings of the international workshop on characterisation and engineering properties of natural soils*, Singapore, Vol. 2, pp. 851–907.

Kovacevic, N., Hight, D. W. & Potts, D. M. (2004). Temporary slope stability in London Clay: back-analyses of two case histories. In *Advances in geotechnical engineering: The Skempton Conference* (eds R. J. Jardine, D. M. Potts and K. G. Higgins), Vol. 3, pp. 1–14. London, UK: Thomas Telford.

Moffat, A. I. B. (2002). The characteristics of UK puddle clays: a review. In *Reservoirs in a changing world*, (ed. P. Tedd), pp. 581–601. London, UK: Thomas Telford.

Penman, A. D. M. (1986). On the embankment dam. *Géotechnique* **36**, No. 3, 303–348, http://dx.doi.org/10.1680/geot.1986.36.3.303.

Potts, D. M. & Zdravkovic, L. (1999). *Finite element analysis in geotechnical engineering: Theory*. London, UK: Thomas Telford.

Potts, D. M. & Zdravkovic, L. (2001). *Finite element analysis in geotechnical engineering: Application*. London, UK: Thomas Telford.

Potts, D. M., Dounias, G. T. & Vaughan, P. R. (1990). Finite element analysis of progressive failure of Carsington embankment. *Géotechnique* **40**, No. 1, 79–101, http://dx.doi.org/10.1680/geot.1990.40.1.79.

Potts, D. M., Kovacevic, N. & Vaughan, P. R. (1997). Delayed collapse of cut slopes in stiff clay. *Géotechnique* **47**, No. 5, 953–982, http://dx.doi.org/10.1680/geot.1997.47.5.953.

Roscoe, K. H. & Burland, J. B. (1968). On the generalised stress-strain behaviour of 'wet' clay. In *Engineering plasticity* (eds J. Heyman and F. A. Leckie), pp. 535–609. Cambridge, UK: Cambridge University Press.

Skempton, A. W. & LaRochelle, P. (1965). The Bradwell slip: a short-term failure in London Clay. *Géotechnique* **15**, No. 3, 221–242, http://dx.doi.org/10.1680/geot.1965.15.3.221.

Tedd, P., Charles, J. A., Holton, I. R. & Robertshaw, A. C. (1997). The effect of reservoir drawdown and long-term consolidation on the deformation of old embankment dams. *Géotechnique* **47**, No. 1, 33–48, http://dx.doi.org/10.1680/geot.1997.47.1.33.

Vaughan, P. R. (1994). Assumption, prediction and reality in geotechnical engineering. *Géotechnique* **44**, No. 4, 573–603, http://dx.doi.org/10.1680/geot.1994.44.4.573.

Vaughan, P. R., Kovacevic, N. & Potts, D. M. (2004). Then and now: some comments on the design and analysis of slopes and embankments. In *Advances in geotechnical engineering: The Skempton Conference* (eds R. J. Jardine, D. M. Potts and K. G. Higgins), Vol. 3, pp. 15–64. London, UK: Thomas Telford.

Watson Hawksley (1990). *Abberton reservoir embankment stability and settlement – review report*. Chelmsford, UK: Essex Water.